Sonic Boom Computations for a Mach 1.6 Cruise Low Boom Configuration and Comparisons with Wind Tunnel Data

Alaa A. Elmiligui[1]
Floyd Wilcox[3]
Linda Bangert[5]

NASA Langley Research Center
Hampton, VA, 23681

Susan E. Cliff[2]
Marian Nemec[4]
Michael J. Aftosmis[6]

NASA Ames Research Center
Moffett Field, CA 94035

and

Edward Parlette[7]
ViGYAN, Inc., Hampton, VA 23666

Accurate analysis of sonic boom pressure signatures using computational-fluid-dynamics techniques remains quite challenging. Although CFD shows accurate predictions of flow around complex configurations, generating grids that can resolve the sonic boom signature far away from the body is a challenge. The test case chosen for this study corresponds to an experimental wind-tunnel test that was conducted to measure the sonic boom pressure signature of a low boom configuration designed by Gulfstream Aerospace Corporation. Two widely used NASA codes, USM3D and AERO, are examined for their ability to accurately capture sonic boom signature. Numerical simulations are conducted for a free-stream Mach number of 1.6, angle of attack of 0.3 and Reynolds number of 3.85×10^6 based on model reference length. Flow around the low boom configuration in free air and inside the Langley Unitary plan wind tunnel are computed. Results from the numerical simulations are compared with wind tunnel data. The effects of viscous and turbulence modeling along with tunnel walls on the computed sonic boom signature are presented and discussed.

Nomenclature

C_p	=	pressure coefficient
DELX	=	distance between model nose and centerline survey probe orifice
DP / P	=	overpressure coefficient = $(P - P_\infty) / P_\infty$
H	=	altitude or distance from model
l, L	=	reference model length, 13.2 in
LBC	=	low boom configuration
P	=	static pressure

[1] Research Aerospace Engineer, Configuration Aerodynamics Branch, M/S 499-1, AIAA Senior Member
[2] Aerospace Engineer, NAS Applications Branch, M/S 258-2, Moffett Field, CA 94035, AIAA Associate Fellow
[3] Aerospace Engineer, Configuration Aerodynamics Branch, M/S 499-1
[4] Senior Research Scientist, Science & Technology Corp., MS 258-5, Moffett Field, CA 94035, Senior Member
[5] Aerospace Engineer, Configuration Aerodynamics Branch, M/S 499-1, Associate Fellow
[6] Aerospace Engineer, Applied Modeling and Simulation Branch, MS 258-5, Associate Fellow
[7] Research Engineer, ViGYAN Research Associates, 30 Research Dr. Hampton, VA 23666/MS 130

P_∞	=	freestream static pressure
Re_L	=	Reynolds number based on the model reference length L
UPWT	=	NASA Langley Unitary Plan Wind Tunnel
WTT	=	wind tunnel test
X	=	axial axis
Xnose	=	model nose axial location
Y	=	vertical axis
Z	=	spanwise axis
α	=	angle of attack
φ	=	off track angle
ϑ_v	=	vertical flow angle
ϑ_H	=	horizontal flow angle
μ	=	Mach angle
ν	=	shearing angle

I. Introduction

A wind-tunnel test (WTT) was conducted to measure the sonic boom pressure signature of a low boom configuration (LBC) designed by Gulfstream Aerospace Corporation (GAC). The WTT was a joint cooperation between GAC and the National Aeronautics and Space Administration (NASA) Langley Research Center (LaRC)[1,2]. The WTT was conducted in the NASA Langley Unitary Plan Wind Tunnel (UPWT) at free-stream Mach numbers of 1.6 and 1.8. The Reynolds number (Re_L), at both Mach numbers, was 3.85×10^6 based on the model reference length. Sonic-boom pressure signatures, surface pressures, model normal force and pitching moment were measured at distances that ranged from 0.5 to 1.7 body length. The test was conducted as part of the Supersonic Cruise Efficiency – Airframe element of the NASA Fundamental Aeronautics Program Supersonics Project. The objective of the Supersonic Cruise Efficiency element is to improve aerodynamic design and analysis capability for highly efficient, supersonic vehicles. The primary technical challenge of the Supersonic Cruise Efficiency element is to develop robust CFD-based methods for rapid design and analysis of supersonic cruise aircraft that are highly efficient, and have low sonic boom. The test was divided into two parts. In the first part, GAC conducted a WTT to measure the sonic boom signature on a LBC. At the end of the test, after all sonic boom measurements were completed, flow Schlieren images were acquired. In the second part of the test, NASA conducted a brief study to determine the effect of boundary layer transition grit on the measured sonic boom signature of the LBC and flow visualization study. A follow up WTT was also conducted at NASA Ames research center to measure the sonic boom signature of the LBC[3].

Computational fluid dynamics (CFD) analysis was also conducted on the LBC[4-7]. Comparison of the computed low boom signature to WTT data showed good agreement for forward part of signature, but less favorable agreement for the aft part of the signature. CFD analysis of the sonic boom pressure signatures remains quite challenging[4-8]. Specialized grids that place grid points within the zone of influence of the sonic boom disturbance or solution-adaptive methods are typically applied to obtain accurate solutions. The authors have recently evaluated methods that use domain rotation of Cartesian grids, developed knowledge-based grid refinement EASS (Elliptical/Annular Swept Sector) techniques for tetrahedral meshes[9], tetrahedral-based grid methods that employs projected Mach cone aligned prism cells (MCAP)[7], and stretching and shearing methods[10] (SSGRID methodology) from seeded tetrahedral grids.

In the present paper, the effects of viscous and turbulence modeling along with the tunnel wall effects on the computed sonic boom signature are evaluated. The flow around the LBC in free air as well as in the UPWT is computed and compared to wind tunnel data. Numerical simulations are conducted for a free-stream Mach number of 1.6, angle of attack of 0.3, h/L = 1.7, and Reynolds number of 3.85×10^6. The CFD codes used in the study were Unstructured Mesh Three Dimensional (USM3D)[11-12] solver and the Adjoint Error Optimization system (AERO)[13-16]. USM3D is a tetrahedral cell-centered, finite volume Euler and Navier-Stokes (N-S) flow solver and provided inviscid, laminar and turbulent flow simulations of the LBC in free air. AERO extends the capabilities of NASA's inviscid, embedded-boundary Cartesian mesh solver, Cart3D, to include adjoint-based error estimation and automatic mesh refinement. It has been verified and validated over a broad range of problems, including supersonic and low-boom studies.[13] AERO provided solutions for the LBC model inside the NASA Langley 4X4 UPWT as well as in free air. The results of this study will help address the issue of tunnel affects and viscous modeling on the

measured supersonic boom signature. Comparison of the computed low boom signature and measured wind tunnel data will be presented and discussed.

The organization of this paper is as follows: (1) a brief description of the wind tunnel test and data reduction (2) descriptions of the CFD codes, USM3D and AERO, used in the study, (3) presentation of the numerical results along with discussion and comparison to wind tunnel data and (4) concluding remarks.

II. Unitary Plan Wind Tunnel Test

A. Unitary Plan Wind Tunnel (UPWT)

The wind tunnel test was conducted in the low Mach number test section of the UPWT, which is a continuous flow, variable pressure supersonic wind tunnel with two test sections. A complete description of the facility along with test section calibration information is contained in reference 17. The test section is approximately 4 ft square and 7 ft long. The nozzle leading to the test section consists of an asymmetric sliding block, which permits continuous variation of Mach number from 1.50 to 2.90 in the low Mach number test section (test section 1). The WTT was conducted at Mach numbers of 1.6 and 1.8 and at a Reynolds number of 3.85×10^6. Figure 1 shows a photograph of the model mounted in the test section. In the present paper, the flow inside the nozzle and test section was computed and compared to WTT data at a Mach number of 1.6, angle of attack of 0.3º and Reynolds number of 3.85×10^6. This set of run conditions will be used throughout this paper.

B. Low Boom Model and Pressure Measuring Probes

A schematic of the low boom configuration model designed by GAC is shown in Figure 2. The model reference, area, chord and span are 8.64 in^2, 2.1029 in. and 4.3594 in., respectively. Further details about the model can be found in references 1 & 2. A telescoping nose is a key identifying feature of the LBC. It was designed to replace a single nose shock with small controlled pressure oscillations to reduce the sonic boom loudness level. The model is mounted to a blade shaped sting designed by GAC. The sting is mounted to the upper surface of the model to minimize interference with sonic boom signature.[18] The top mounted sting is a state-of-the-art approach that permits accurate measurements of the empennage flow field. This mounting system was designed to simulate flight and was carefully designed to have no effect on the pressure signature.

The low boom signature was measured with four static pressure probes mounted on the west tunnel wall door blank. Figure 3 shows top and side views of reference and survey probes as mounted in the UPWT. One probe served as a reference probe and measured the free stream static pressure and remained in a fixed position. All three survey probes were in the same vertical plane and were mounted on an axial traverse mechanism. The relative distance between all four probes and their relative location in the tunnel is shown in Figure 3. The survey probes were mounted on a traverse so that the probes can be moved longitudinally in the tunnel. Figure 4 shows a photograph of the traverse and survey probes mounted in the tunnel. The reference probe pressure was used as the reference for all of the survey probes. In the computational model, the reference probes were not modeled however the pressure signature was extracted from the computed flow field at the exact normal distance from the tunnel wall as the survey probes. It should also be mentioned that in the computational model the LBC was facing the east wall while in the WTT, LBC was facing the west wall. This should not affect the quality of the simulation because the flow in the tunnel is symmetric.

C. Wind Tunnel Test Procedure and Data Reduction

A typical sonic boom pressure signature run consisted of first adjusting the sonic boom angle of attack mechanism so that a given normal force was obtained on the model. Using the tunnel model support system, the model nose was laterally positioned a specified distance, h, from the on-track (centerline) survey probe. Initially, the model was located so that the nose shock was downstream of the survey probes. The model was then moved forward in 0.125-inch increments while the model pressure signature data were obtained from the reference and survey static pressure probes. As the model was moved forward during the run, the model normal force would vary because of flow gradients within the test section. Data were acquired in a move/pause mode of operation. For each pressure signature run, the model was moved approximately 24 inches. The CFD analysis was intended to mimic this test procedure however due to computation and time constrains only four axial locations were computed and compared to wind tunnel data.

The WTT data was acquired over a period of 8 days at various times during the day. On-track and off-track sonic-boom pressure signatures, surface pressures, model normal force and pitching moment were measured at distances that ranged from 0.5 to 1.7 body length for a range of Mach numbers from 1.6 to 1.8, for three angles of

attack (-0.25°, 0.25°, 0.69°). The tunnel air dew point was maintained below -20°F (at atmospheric pressure) to minimize water vapor condensation. Details of the tunnel running conditions used during this test can be found in reference 1. The effects of Mach number, h/L, angle of attack, survey probe position, and boundary layer transition grit on the sonic boom signature are presented in reference 1.

Wind tunnel data show that the overpressure coefficient standard deviations remained relatively constant over the length of the test. Figure 5 shows data repeatability for the wind tunnel test. The first five data points in each pressure signature run were used to adjust the signatures to account for static pressure variation within the test section. This correction was made because of the static pressure variations within the tunnel test section. More information on the data reduction can be found in references 1 and 2. Figure 5 illustrates the salient features of the low boom signature data; the pressure peaks from the nose tip and the four nose segments are clearly visible in the plot. Figure 6 shows three sonic boom signature runs that were acquired back-to-back, while the position of the survey probes was varied by 2 inches. Ideally, these runs should be as repeatable as the repeat runs shown in Figure 5. However, the results indicate that there is additional scatter in the data. The variation in tunnel flow conditions as a function of location within the test section is a factor in the additional data scatter.

During the WTT, sublimation tests were conducted to determine the size and location of boundary layer grit that would transition the boundary layer flow from laminar to turbulent. The transition strips consisted of sand grit sparsely sprinkled in a lacquer film and are shown in Figure 7. The effect of boundary layer grit on the sonic boom signatures for M = 1.60 is shown in Figure 8. The primary affect of the boundary layer grit is seen downstream of the wing expansion. Turbulent flow over the model wing does not significantly affect the peak pressures generated by the wing. The grit located on the model nose does not create a noticeable pressure peak, whereas, the wing boundary layer grit does show a compression, expansion, and re-compression at DELX ≈ 32 inches.

III. General Description of Computational Methods

The two NASA software systems used for the computational analysis were the Tetrahedral Unstructured Software System (TetrUSS)[19] and AERO[20] package. GAC delivered the as built surface definition of LBC in Catia part format. NASA LaRC Geometry Laboratory used the Catia files to prepare and deliver a design surface definition in a PLOT3D unformatted, double precision file format. The design sting surface definition was then added to LBC. The sting mounted on the as built surface definition for the LBC is shown in Figure 9. TetrUSS and AERO used the same surface mesh. The codes and the boundary conditions are described in the next section.

A. Tetrahedral Unstructured Software System (TetrUSS)

TetrUSS was developed at NASA Langley Research Center and includes; a model/surface grid preparation tool (GridTool), field grid generation software (VGRID, POSTGRID) and a computational flow solver (USM3D). The USM3D flow solver has internal software to calculate forces and moments. Additionally, the NASA LaRC-developed code USMC6[21] was used for analyzing the solutions.

TetrUSS Computational Grids

For the LBC in free air, inviscid and viscous volume grids were generated by the Mach Cone Aligned Prism (MCAP) approach[7]. A refined unstructured grid within a cylinder in the near field is followed by projection of the surface faces on the cylindrical boundary in the radial direction with a series of prism layers to the far field. The MCAP method maintains highly refined grid spacing in the axial direction throughout the entire mesh, and allows control of the radial stretching and shearing (to align with the Mach cone angle around the aircraft). Projecting each triangular face forms a prism that is then sheared to align with the Mach angle. More details about MCAP method can be found in reference 7. The inviscid grid consisted of 72 million cells while the viscous grid had 130 million cells. Figure 10 shows a planar cut showing the USM3D grid distribution for the viscous grid. Some guidelines for grid generation included the requirement for surface cell size to be small enough to resolve features and curvature of the LBC. Proper boundary layer spacing was used to ensure y+ remains less than or equal to 1 for the selected free stream Mach and Reynolds numbers. It is beneficial to start aligning the mesh as close to the body as possible for accurate sonic boom pressure signatures even at distances less than one body length.

Surface patches were created on the configuration in GridTool[22] using a PLOT3D surface definition of the geometry. Sources were placed throughout the domain to cluster cells and accurately capture configuration characteristics. The output from GridTool was used to automatically generate the computational domain with the VGRID unstructured grid generation software. VGRID uses an Advancing Layers Method to generate thin layers of

unstructured tetrahedral cells in the viscous boundary layer,[23] and an Advancing Front Method to populate the volume mesh in an orderly fashion.[24] POSTGRID was used to close the grid by filling in any gaps that remain from VGRID. POSTGRID is automated to carefully remove a few cells surrounding any gaps in the grid and precisely fill the cavity with the required tetrahedral cells. Volume grids generated inside the tunnel failed to resolve sonic boom signature. The authors are currently working on refining this process of grid generation to be able to capture sonic boom in a computational mesh that models the inside of a wind tunnel. Figure 11 shows schematic of LBC inside the UPWT. Figure 12 shows a plane of the inviscid grid distribution inside UPWT for the USM3D grid with 76 million cells.

TetrUSS FlowSolver USM3D

The flow solver for the TetrUSS software package is USM3D. USM3D is a tetrahedral cell-centered, finite volume Euler and Navier-Stokes (N-S) method. The USM3D flow solver has a variety of options for solving the flow equations and several turbulence models for closure of the N-S equations.[27-28] A script program, written as part of the Ares V project guidelines development, was used to automatically setup input parameters for choosing the proper flux scheme and CFL numbers based on the desired Mach number for each case.[29] For the current study, Roe's flux difference splitting scheme was used and CFLmax was set to 20. Flux limiters are used within CFD codes to preclude oscillations due to shocks and discontinuities by limiting the values of the spatial derivatives. Typically, a flux limiter is required for supersonic flows and not for subsonic flow computations. For the present study, at the start of a new solution, the USM3D code ran with first order spatial accuracy for 10000 iterations, and then the code automatically switched to second order spatial accuracy. Figure 13 shows convergence history for the LBC in free air using SA turbulence model. Three turbulence models were investigated in this study. The SA turbulence model was the default turbulence model used, however when solution failed to capture the peak and aft part of the signature, the shear stress transport (SST) model and KE turbulence models were used. Details of the implementation of the three turbulence models within USM3D can be found in reference 28.

B. AERO Package

AERO is a high-fidelity design package for conceptual and preliminary aerodynamic design that uses Cartesian meshes. It allows users to perform automated CFD analysis on complex geometry. The AERO package computes a reliable approximation of user-selected outputs, such as pressure signatures; through use of adjoint error estimation and automatic mesh refinement.

AERO Computational Grids

The AERO package has an internal module to generate the volume grid called Cubes.[25] The computational mesh consists of regular hexahedra everywhere, except for a layer of body-intersecting cells, or cut-cells, adjacent to the boundaries. AERO uses adjoint-weighted residual error-estimates to drive mesh adaptation. Once a user specifies outputs of interest (lift, drag, etc.) with a corresponding error tolerance, AERO automatically refines meshes to drive the remaining numerical errors in the outputs below the requested tolerance.[25] In the current study, the goal was the evaluation of the sonic boom pressure signature and hence function of interest was selected as a pressure coefficient 'sensor' along a line in the domain given by:

$$J = \int (DP / P)^2 \, ds$$

Figure 14 shows the symmetry plane of the AERO grid colored with cp for LBC in free air. The grid had 47 million cells after eleven levels of adaption. Two co-linear equally weighted line sensors were placed at 1.7 body lengths below the model. The second line sensor was used to emphasize the nose spike shocks and provide a solution with less mesh points. The LBC in the UPWT was evaluated at four axial locations, at x_{nose} of -5, 0, 5, and 10 inches. Four grids were generated in the order of 110 million cells after 13 levels of adaption. The AERO approach relies on the solution of the adjoint equation and provides error estimates that can be used to both improve the accuracy of the functional and guide a mesh refinement procedure. Table 1 gives the initial and final cell count for the grids generated by AERO.

Table 1. Cell Count For The Various Grids Used In AERO Calculation

Case	Initial Mesh cell Count	Final Mesh cell count	Adaption Level
Model in Free Air	59340	47,589,164	11
Empty Tunnel	20,857	113,708,596	13
Model @ x = -5	20,857	111,678,140	13
Model @ x = 0	20,857	106,120,140	13
Model @ x = 5	20,856	116,158401	13
Model @ x = 10	20,856	116,26,6040	13

AERO Flow Solver CART3D

CART3D is the current flow solver being released with the AERO package. It is a scalable, multilevel, linearly exact upwind solver and uses domain-decomposition to achieve very good scalability[20]. CART3D is very tightly integrated into AERO package and all of the automation tools are built around it. The spatial discretization uses a cell-centred, second-order accurate finite volume method with a weak imposition of boundary conditions. The flux-vector splitting approach of van Leer is used in conjunction with the Barth-Jespersen limiter. Convergence to steady-state is obtained via a five stage Runge-Kutta scheme, multigrid and a domain decomposition scheme for parallel computing. Further details are given in references.[13-16]

C. Initial and Boundary Conditions

For the model in free air and inviscid flow simulations, an inviscid aerodynamic surface boundary condition (BC) was used on all solid surfaces. The supersonic inflow BC was used at the domain inflow face and the extrapolation BC was used at the downstream outflow face of the domain. The characteristic inflow and outflow BC was used along the far field, lateral faces of the outer domain. For USM3D viscous simulation the no-slip viscous BC was used on all solid surfaces of the LBC. For the model inside the tunnel simulations, AERO utilized a prescribed surface BC at the inlet and exit surfaces, while USM3D used the jet BC at the inlet boundary and full extrapolation, supersonic outflow BC at the exit.

IV. Results

The flow field around the LBC was computed using TetrUSS and AERO for a free-stream Mach number of 1.6, $\alpha = 0.3$ to match WTT force coefficients, and a Reynolds number of 3.85×10^6. The computational results of the LBC in free air will be presented first, followed by the results for the empty tunnel and LBC in the UPWT.

A. LBC in Free Air

For the free air simulation, AERO provided an invisid simulation on a final grid of 47 million cells after eleven levels of adaption. Two co-linear equally weighted line sensors were placed at 1.7 body lengths below the model. The second line sensor was used to emphasize the nose spike shocks and provide a solution with less mesh points. USM3D was used to obtain an inviscid solution on a 72 million-cell grid. Figure 15 shows upper surface pressure distribution using USM3D inviscid simulation. **Figure** 16 and Figure 17 show symmetry plane grid colored by pressure coefficient and overlaid constant pressure lines for a USM3D solution of the LBC in free air at M=1.6 and $\alpha = 0.3°$. The signature was sampled at 1.7 body lengths below model. Experimental data with USM3D inviscid simulation and CART3D is shown in Figure 18. There is good agreement with experiment in the forward portion of the pressure signature but poor agreement in the aft region. Similar behavior was reported by other LBC researchers[4-9]. In an attempt to better capture the aft part of the signature and to investigate the effect of viscous modeling on the prediction of the sonic boom signature, four USM3D viscous simulations were conducted. A Navier-Stokes near-field grid was generated using VGRID and then the prism mesh was attached in a similar fashion as the Euler grids. The original grid had 52 million cells. Figure 19 shows the symmetry plane solution near the configuration. The viscous solution with USM3D is compared with experimental data in Figure 20. The viscous solution on the 53 million cell grid appears to be capturing the entire forward signature through the expansion that crosses the y=0 axis. The aft signature does not agree well with the experimental results due to insufficient grid used near the aft region of the model. To better capture the aft part of the signature, a 130 million-cell grid was generated and used to adequately model viscous and turbulence effects. The finer grid captures more details in the aft part of

the signature and is closer to WTT data, which emphasizes the importance of the grid density in capturing low boom signatures.

Four viscous solutions were obtained on the fine grid; one laminar and three fully turbulent simulations. The three turbulence models used to model turbulence were: the standard k-ε model (KE), the Spalart-Allmaras model (SA) , and the Menter SST model. Figure 21 shows comparison of USM3D viscous solutions and the UPWT data for the model in free air. All USM3D calculations accurately captured nose shocks but had poor agreement in the aft region. The differences in pressure boom signatures from viscous modeling starts to show at X/L=2.5 which corresponds to the region of main compression on the wing. Figure 22 shows USM3D KE symmetry plane solution near the configuration. All models underestimated the strength of the wing expansion and recovery, however the KE model signature provided the closest correlation to the UPWT data. Figure 23 and Figure 24 compare experimental off track pressure signatures with USM3D off track viscous signatures. The ability to capture the nose shock as well as shown here is a significant accomplishment because the MCAP computational mesh was constructed to radially align on-track and off-track[9]. The reason for the poor correlation with UPWT in the aft part of the signature is unknown and might be attributed to the effects from the wind tunnel flow-field on the model. In the next section attempts to evaluate wind tunnel effects on the signature boom by modeling the LBC inside the wind tunnel are made.

B. Empty Tunnel

Empty UPWT simulations were performed with USM3D and CART3D. These calculations were conducted to evaluate flow angularity and quality of the flow inside the tunnel. Figure 25 shows a cross section view of the grid in the tunnel colored by Mach contours. The flow angles measured in the horizontal plane (ϑ_v) and (ϑ_H) are shown in Figure 26 for the USM3D code using the SA turbulence model. The flow angle ϑv varies by less than 1° degree in the test section and less than 0.4° in the horizontal plane (z = 0 plane), while ϑ_H varies by less than 0.05°. The computed flow angularity, ϑ_H and ϑv, are in good agreement with tunnel calibration results[17]. The empty tunnel flow was also computed by AERO and the grid after 13 cycles of adaption had around 114 million cells. The initial mesh had 20,857 cells. Two co-linear equally weighted line sensors were placed at 10 in from tunnel wall.

C. LBC in UPWT

During the WTT, the model was moved forward in 0.125 inch increments while the model pressure signature data were obtained from the reference and survey static pressure probes. Data were acquired in a move/pause mode of operation. For each pressure signature run, the model was moved approximately 24 inches. The CFD analysis was intended to mimic the WTT procedure so CFD signatures at four axial locations were computed and compared to wind tunnel data. Furthermore, the WTT pressure probes were at a distance of 10 inches from the wall and therefore, the line sensors were placed at the same distance for the CFD calculations.

TetrUSS (USM3D)

USM3D simulations of flow around LBC in the wind tunnel was a challenging task due to difficulties in generating a suitable computational grid. As discussed in the previous section, preserving shock waves for multiple body lengths without dissipation requires a fine stretched grid that is aligned with the direction of the shock. This helps reduce diffusion of the shock in computational domain and thus enable the numerical scheme to accurately predict the sonic boom signature away from the body. VGRID and POSTGRID had difficulty producing grids with high stretching ratios inside the wind tunnel because the advancing-front algorithm as implemented is not stable for such stretching. The problem is even more difficult when large volumes are required in order to capture shocks away from the vehicle. Figure 27 shows cross section view of the grid colored by DP/P contours for the LBC inside the UPWT at Mach=1.6, h/l = 1.7, and α=0.3° for the USM3D inviscid solution on a 74 million cell grid. The arrow in the figure points to the location of the pressure probe in the tunnel. The grid was deemed too coarse for this sonic boom calculation. Currently, work is being pursued to generate a grid similar in quality to the grid generated by MCAP method. In a parallel effort, authors are also investigating using Chimera overset-grid capability within USM3D as well as hybrid methods to compute flow around the LBC in the tunnel.

AERO (CART3D)

The flow computations from CART3D of the LBC in the UPWT were evaluated at four axial locations, at x_{nose} of -5, 0, 5, and 10 inches, in addition to the empty tunnel run. All 4 solutions achieved thirteen levels of adaption. Table 1 provides the cell count for each of the grids used in this study. Figure 28 shows the pressure contours after thirteen adaptation cycles for the model at x = 5 inches solution. The refinement pattern is driven by the features of

the adjoint solution. Two co-linear equally weighted line sensors were placed at 1.7 body lengths below the model. The second line sensor was used to emphasize the nose spike shocks and provide a solution with less mesh points.

Figure 29 shows a comparison between the computed sonic boom signatures of the LBC in the UPWT at the four x locations with the WTT data. AERO CART3D results captured nose shocks and the salient features of low boom signature. The authors are developing alternative adapting strategies to capture the aft part of the shock signature. The boom signature changes in shape as the model moves inside tunnel, an expected result due to pressure variation in the tunnel. Future work would involve generating complete data set and comparing CFD results with WT data as well as exploring new strategies for adaption.

Schlieren Flow Visualization

After all sonic boom measurements were completed in the WTT, Schlieren photographs of the model were obtained. During this test, the Schlieren system knife-edge was oriented approximately parallel to the free-stream flow to highlight density gradients in the vertical direction. For this knife-edge orientation, increasing density gradients in the upward direction appear as white areas in the photographs. Figure 30 shows comparison between UPWT Schlieren photograph and computed density gradients for both AERO (CART3D) and USM3D solutions of the LBC inside UPWT at a Mach number of 1.6. The vertical black lines in the UPWT Schlieren photograph are the test section window support bars. The USM3D computed density gradients faded out as we moved away from LBC while the AERO system preserved signature features. Although USM3D accurately captured sonic boom signature in free air, the model in wind tunnel grid diffused the sonic boom signature. This emphasizes the importance of creating fine, stretched and shock aligned grid cells in order to capture sonic boom signatures. The AERO package automatically provides this quality of cells because it relies on the solution of an adjoint equation and provides error estimates that can be used to both improve the accuracy of the functional and guide a mesh refinement procedure.

V. Conclusion

A wind tunnel test was conducted by Gulfstream Aerospace Corporation to measure the sonic boom signature of a low boom configuration in the Langley Unitary Plan Wind Tunnel (UPWT) at Mach numbers of 1.60 and 1.80. Two widely used NASA codes, TetrUSS and AERO were used to compute sonic boom signature of the low boom configuration (LBC) in free air as well as in the wind tunnel at a free-stream Mach number of 1.6, an angle of attack of 0.3°, and a Reynolds number of 3.85×10^6. Inviscid, laminar and turbulent solutions were computed with USM3D using the SA, SST and KE turbulence models. The effects of viscous and turbulence modeling along with the presence of the wind tunnel wall on the computed sonic boom signature were presented. On- and off-track sonic boom signatures were computed and compared to wind-tunnel test data. Comparison showed that sonic boom signature captured by KE model was the closest to the WTT data. Mach cone aligned prism cells provided accurate on-track and off-track pressure signatures. Fine, stretched, and shock aligned grids are a key parameter in capturing low boom signature.

The AERO package successfully computed low boom signature of the LBC in free air and at four axial locations in the tunnel. This work proved the ability of the adjoint-based mesh adaptation method to guide refinement and control discretization errors in inviscid simulations around complex geometries in the tunnel. Authors are currently involved in generating a complete data set of sonic boom wind tunnel test that was conducted in the NASA Ames 9X7 Foot Supersonic Wind Tunnel. New strategies for adaption are being considered. Future work to incorporate the Mach cone aligned prism (MCAP) cells program into a grid generation tool suite developed at NASA Langley Research Center, to generate viscous near body grids with cylindrical boundaries is being planned. The use of USM3D Chimera overset-grid capability in TetrUSS, to overcome difficulties of generating fine-stretched grids inside tunnel grids, is also being considered.

Acknowledgments

The authors would like to thank Donald A. Durston and Scott D. Thomas of NASA Ames Research Center for their valuable comments and long hours of discussion through out the course of this work. Authors thank Norma Farr and Michael Wiese of the Geometry Laboratory at NASA Langley Research Center for developing surface and volume grids.

References

1. Wilcox, F. J.; and Elmiligui, A. A.: "Experimental Sonic Boom Measurements on a Mach 1.6 Cruise Low-Boom Configuration," NASA TM to be published.
2. Wayman, T., Howe, D., Waithe, K., Bangert, L., and Wilcox, F.: "Near Field Acoustic Test on a Low Boom Configuration in Langley's 4 x 4 Wind Tunnel," 29th AIAA Applied Aerodynamics Conference, Honolulu, HI, June 2011.
3. Durston, D. A., Cliff, S. E., Wayman, T., Merret J., Elmiligui, A., and Bangert, L.: "Near-Field Sonic Boom Test on Two Low-Boom Configurations Using Multiple Measurement Techniques at NASA Ames," 29th AIAA Applied Aerodynamics Conference, Honolulu, HI, June 2011.
4. Carter, M. B., Campbell, R., and Nayani, S.: "USM3D Analysis of a Low Boom Configuration," 29th AIAA Applied Aerodynamics Conference, Honolulu, HI, June 2011.
5. Howe, D.: "Hybrid CART3D/OVERFLOW Near-Field Analysis of a Low Boom Configuration with Wind Tunnel Comparisons," 29th AIAA Applied Aerodynamics Conference, Honolulu, HI, June 2011.
6. Park, M.: "Low Boom Configuration Analysis with FUN3D Adjoint Simulation Framework," 29th AIAA Applied Aerodynamics Conference, Honolulu, HI, June 2011.
7. Cliff, S., Elmiligui, A., Campbell, R., and Thomas, S.: "Evaluation of Refined Tetrahedral Meshes with Projected, Stretched, and Sheared Prism Layers for Sonic Boom Analysis," 29th AIAA Applied Aerodynamics Conference, Honolulu, HI, June 2011.
8. Carter, M. B., and Deere, K. A.: "Grid Sourcing and Adaptation Study Using Unstructured Grids for Supersonic Boom Prediction," AIAA Paper 2008-6595, 2008.
9. Cliff, S., Thomas, S., McMullen, M., Melton, J., and Durston, D.: "Assessment of Unstructured Euler Methods for Sonic Boom Pressure Signatures Using Grid Refinement and Domain Rotation," NASA/TM-2008-214568, September 2008.
10. Campbell, R. L., Carter, M. B., Deere, K. A. and Waithe, K. A.: "Efficient Unstructured Grid Adaptation Methods for Sonic Boom Prediction," AIAA Paper-7327, Honolulu HI, August 2008.
11. Frink, N. T., Pirzadeh, S. Z., Parikh, P. C., Pandya, M. J., and Bhat, M. K.: "The NASA Tetrahedral Unstructured Software System," The Aeronautical Journal, Vol. 104, No. 1040, October 2000, pp. 491-499.
12. Frink, N. T.: "Assessment of an Unstructured-Grid Method for Predicting 3-D Turbulent Viscous Flows," AIAA Paper-96-0292, January 1996.
13. Nemec, M., Aftosmis, M. J., Murman, S. M., and Pulliam, T. H.: "Adjoint Formulation for an Embedded-Boundary Cartesian Method," AIAA Paper 2005–0877, Reno, NV, January 2005.
14. Nemec, M., and Aftosmis, M.: "Adjoint Error-Estimation and Adaptive Refinement for Embedded-Boundary Cartesian Meshes," AIAA Paper 2007-4187, 18th AIAA CFD Conference, Miami FL, June 2007.
15. Nemec, M., Aftosmis, M., and Wintzer, M.: "Adjoint-based Adaptive Mesh Refinement for Complex Geometries," AIAA Paper 2008-0725, January 2008.
16. Aftosmis, M. J., and Berger, M. J.: "Multilevel Error Estimation and Adaptive H-Refinement for Cartesian Meshes with Embedded Boundaries," AIAA Paper 2002-0863, 40th AIAA Aerospace Sciences Meeting and Exhibit, Reno NV, January 2002.
17. Jackson, C. M., Jr., Corlett, W. A., and Monta, W. J.: Description and Calibration of the Langley Unitary Plan Wind Tunnel. NASA TP-1905, 1981.
18. Waithe, K. A.: "Design of a Wind Tunnel Mount for a Low Boom Test" 29th AIAA Applied Aerodynamics Conference, Honolulu, HI, June 2011.
19. TetrUSS Web page: http://tetruss.larc.nasa.gov/usm3d/index.html, May 2011.
20. CART3D Web page: http://people.nas.nasa.gov/~aftosmis/cart3d, May 2011.
21. Pao, S. P.: "USMC6-TetrUSS Grid and Solution Cutter: A Brief Users' Guide," Version 4, NASA LaRC, September 2010.
22. Samareh, J.: "GridTool, A Surface Modeling and Grid Generation Tool," Proceedings of the Workshop on Surface Modeling, Grid Generation, and Related Issues in CFD Solutions, NASA CP–3291, May 9–11, 1995.
23. Pirzadeh, S.: "Unstructured Viscous Grid Generation by Advancing-Layers Method," AIAA Journal, Vol. 32, No. 8, pp. 1735–1737, August 1994.
24. Pirzadeh, S.: "Structured Background Grids for Generation of Unstructured Grids by Advancing Front Method," AIAA Journal, Vol. 31, No. 2, pp. 257–265, February 1993.
25. Aftosmis, M. J., Berger, M. J., and Melton, J. E.: "Robust and Efficient Cartesian Mesh Generation for Component-Based Geometry," AIAA Paper 97-196.

26. Nemec, M., Aftosmis, M. J., and Wintzer, M.: “Adjoint-based Adaptive Mesh Refinement for Complex Geometries," AIAA 2008-0725.
27. Pandya, M. J., Abdol-Hamid, K. S., and Frink, N. T.: “Enhancement of USM3D Unstructured Flow Solver for High-Speed High-Temperature Shear Flows,” AIAA 2009-1329, January 2009.
28. Abdol-Hamid, K. S., Frink, N. T., Deere, K. A., and Pandya, M. J.: “Propulsion Simulations Using Advanced Turbulence Models with the Unstructured-Grid CFD Tool, TetrUSS,” AIAA 2004-0714, January 2004.
29. Deere, K. A., Elmiligui, A. A, Abdol-Hamid, K.S.: “USM3D Simulations of Saturn V Plume Induced Flow Separation,” AIAA-2011-1055.
30. Jackson, C. M., Jr., Corlett, W. A., and Monta, W. J.: Description and Calibration of the Langley Unitary Plan Wind Tunnel. NASA TP-1905, 1981.
31. Pandya, M.J., Frink, N.T., and Noack, R.W.: “Overset-grid Moving Body Capability in the USM3D Unstructured Flow Solver,” AIAA Paper 2005-5118.

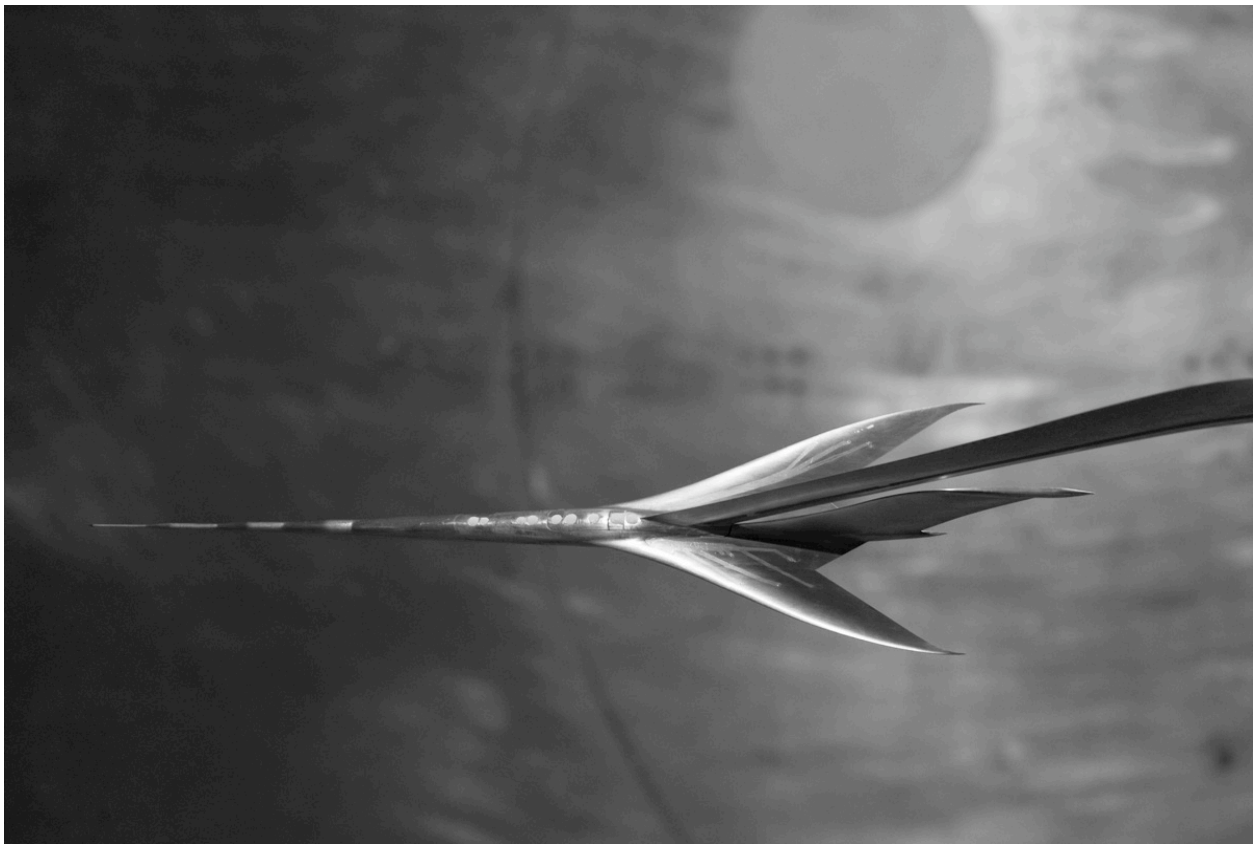

Figure 1. LBC mounted in NASA Langley UPWT.

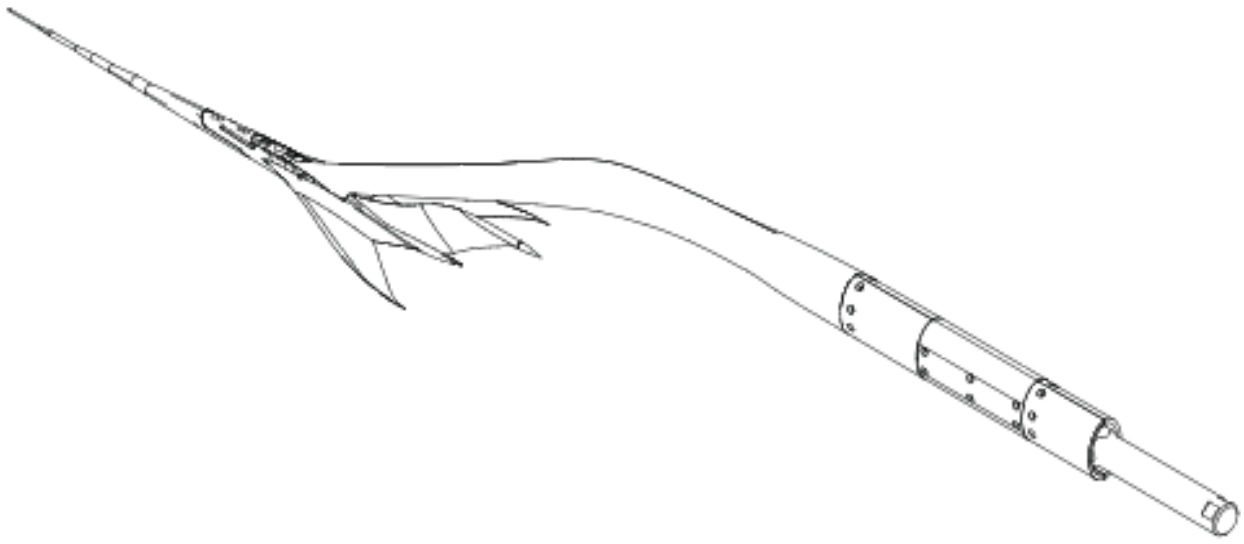

Figure 2. Isometric of low boom configuration and blade sting.

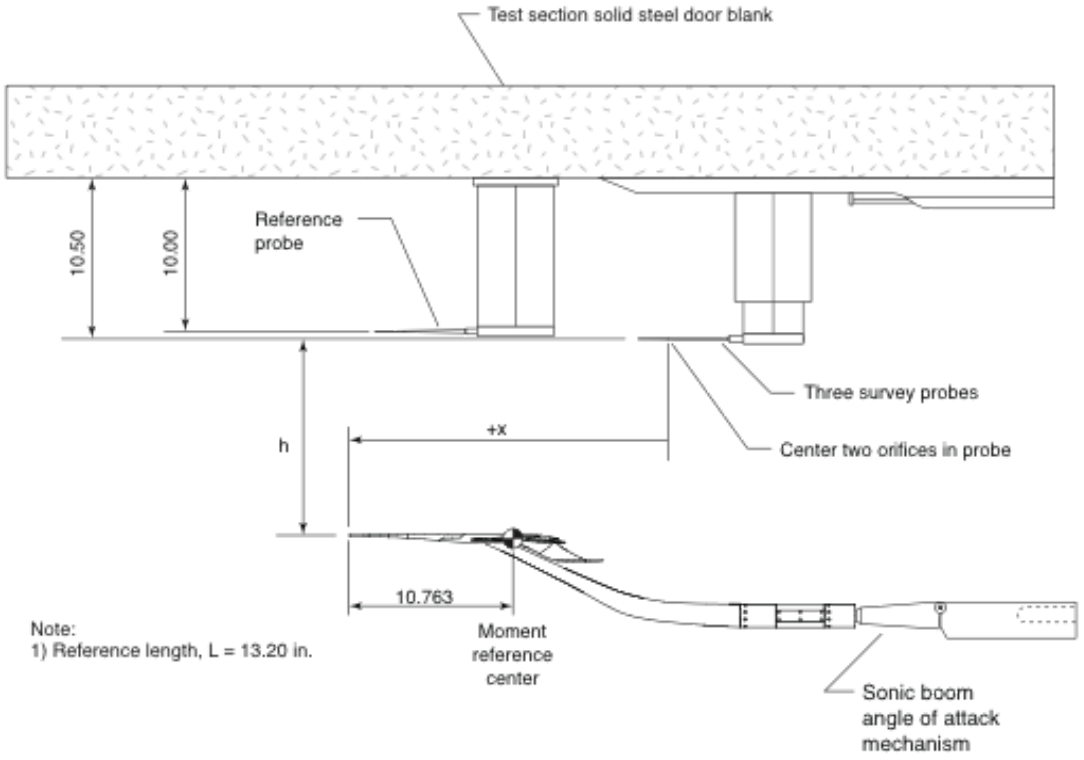

(a) Top View.

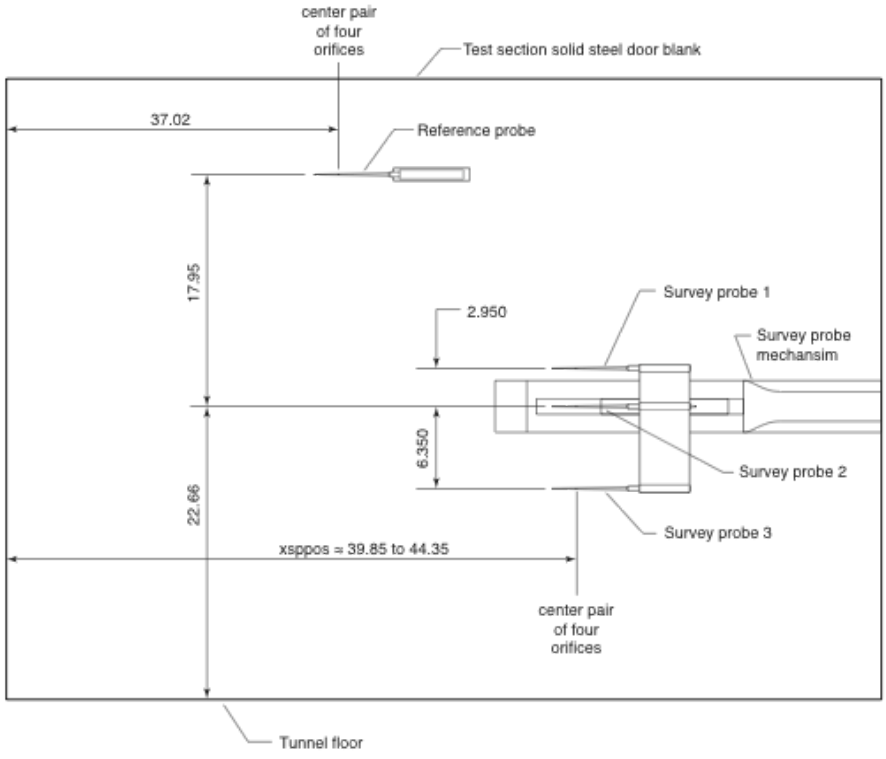

(b) Side View.

Figure 3. Location of reference and survey pressure probes in the UPWT. (All dimensions in inches)

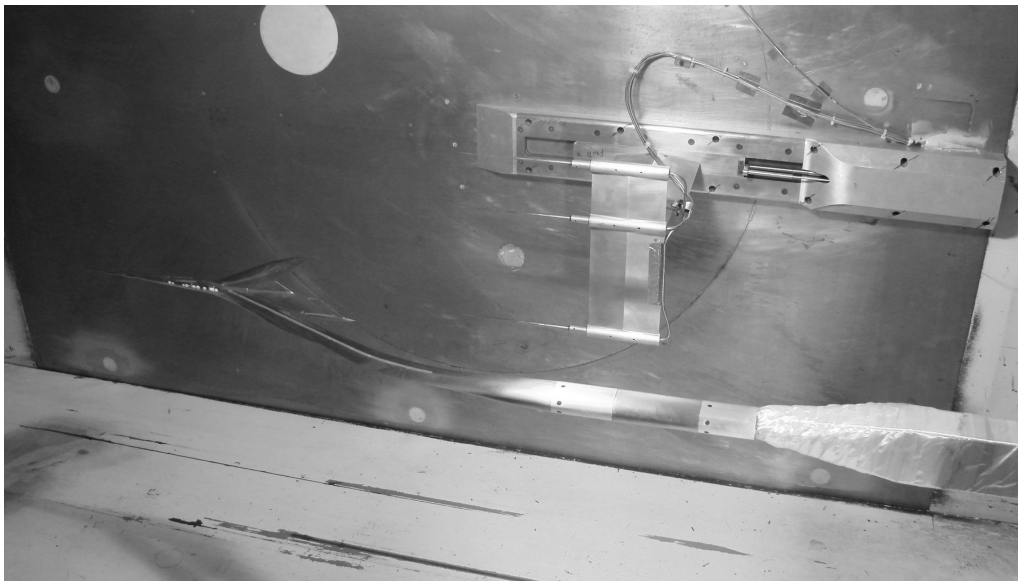

Figure 4. Photograph of the LBC, traverse mechanism, and survey probes mounted in the UPWT.

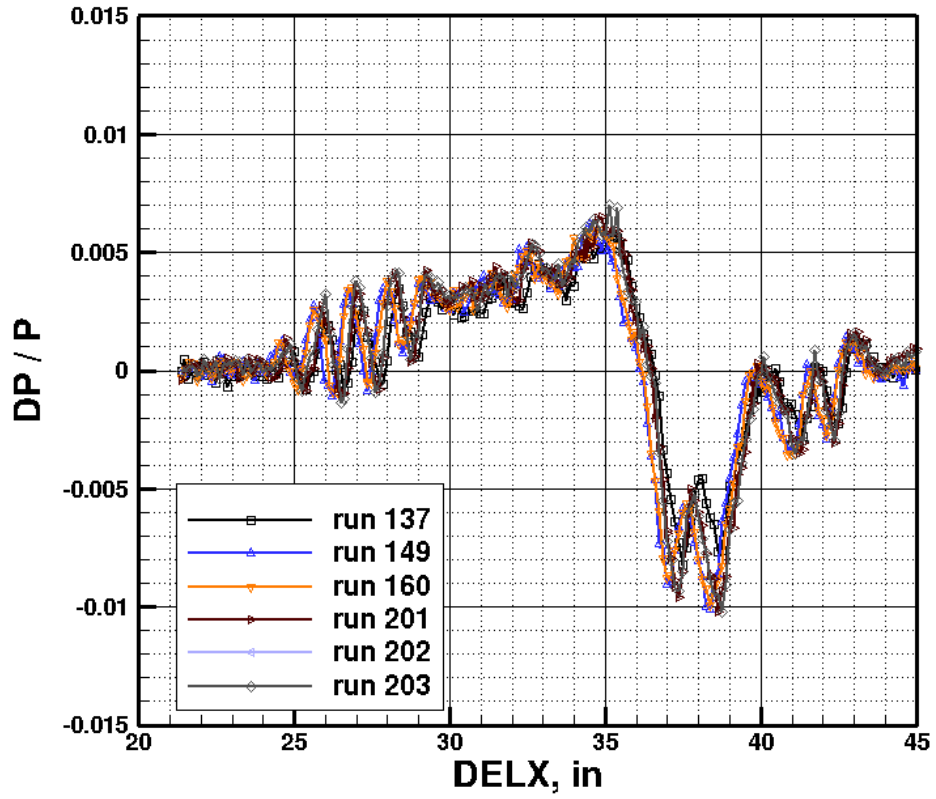

Figure 5. Wind tunnel data repeatability at M=1.6, ∝=0.25°, H/L=1.7, Xnose = 42.35 inches, $Re_L = 3.85x10^6$.

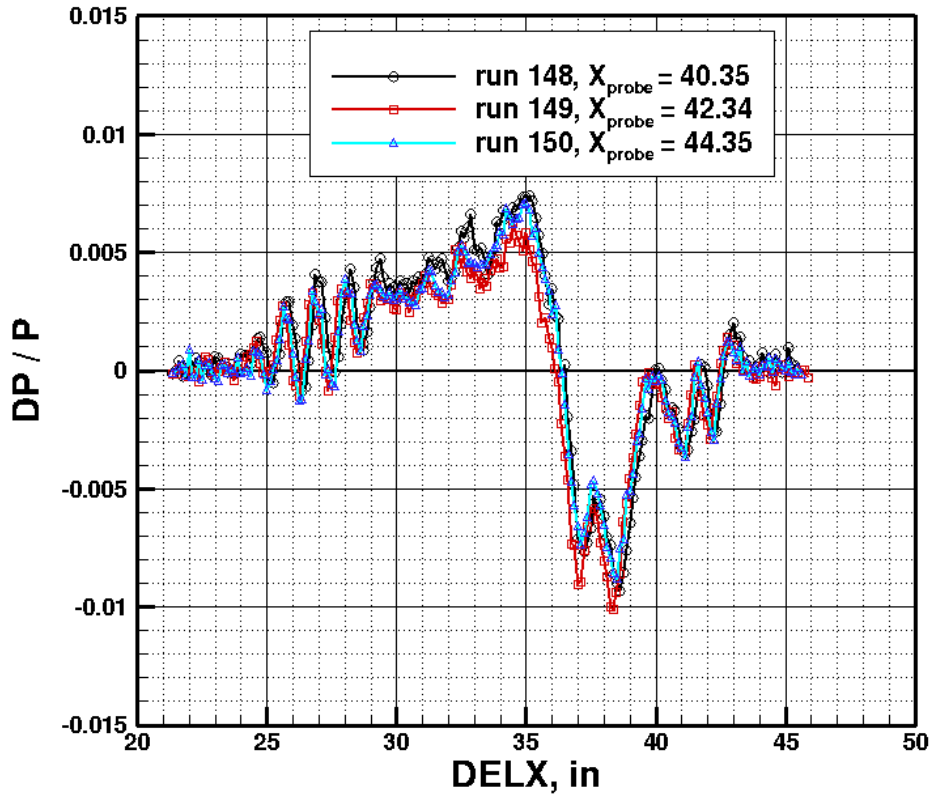

Figure 6. Effect of survey probe position on sonic boom signature at M=1.6, ∝=0.25°, H/L=1.7, $Re_L = 3.85x10^6$.

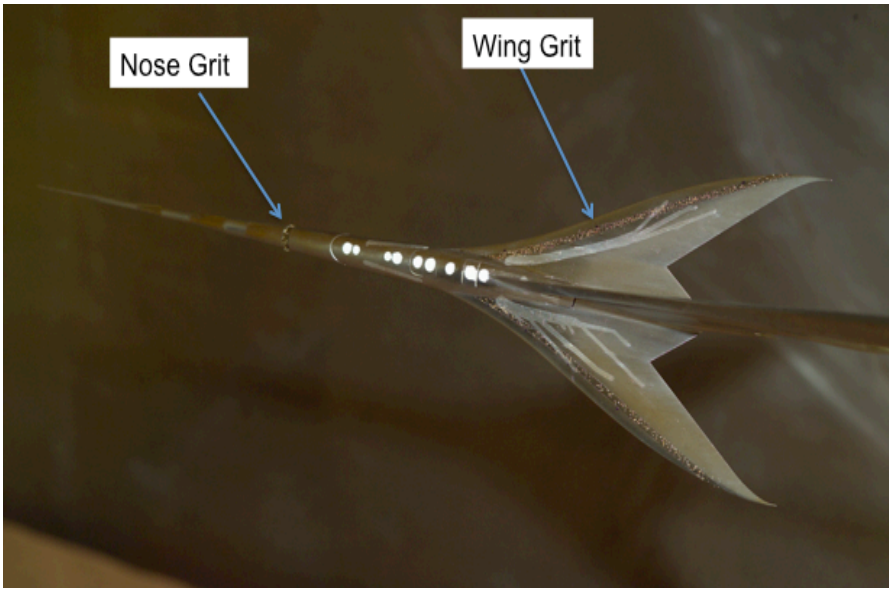

Figure 7. Photograph showing grit location on LBC.

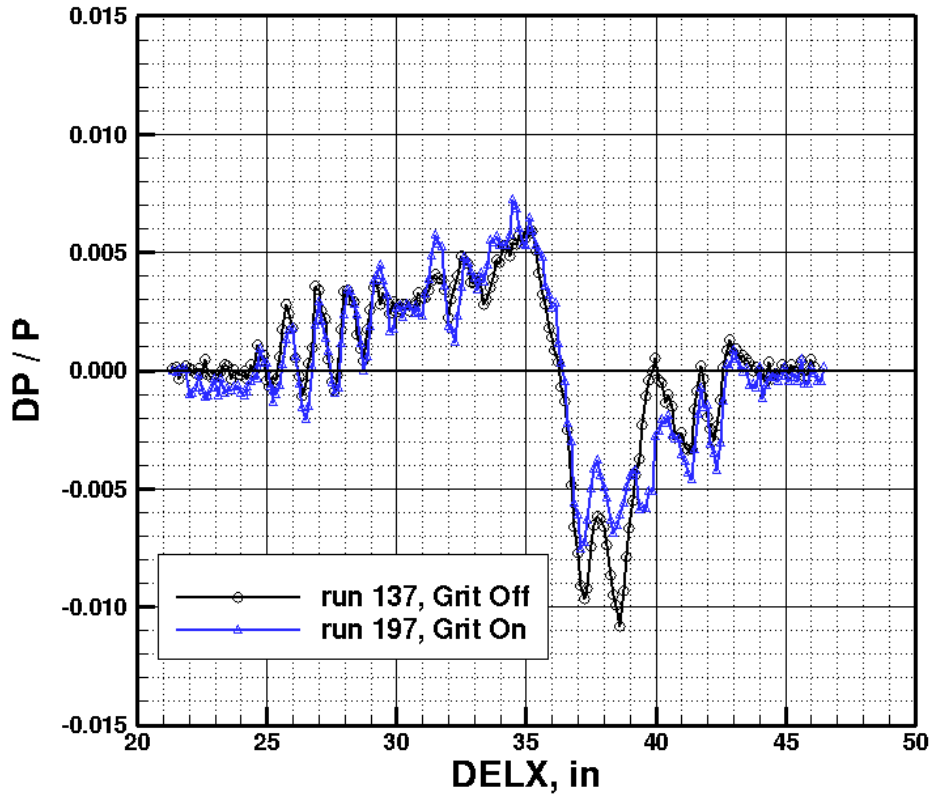

Figure 8. Effect of boundary layer transition grit.

Figure 9. LBC surface mesh.

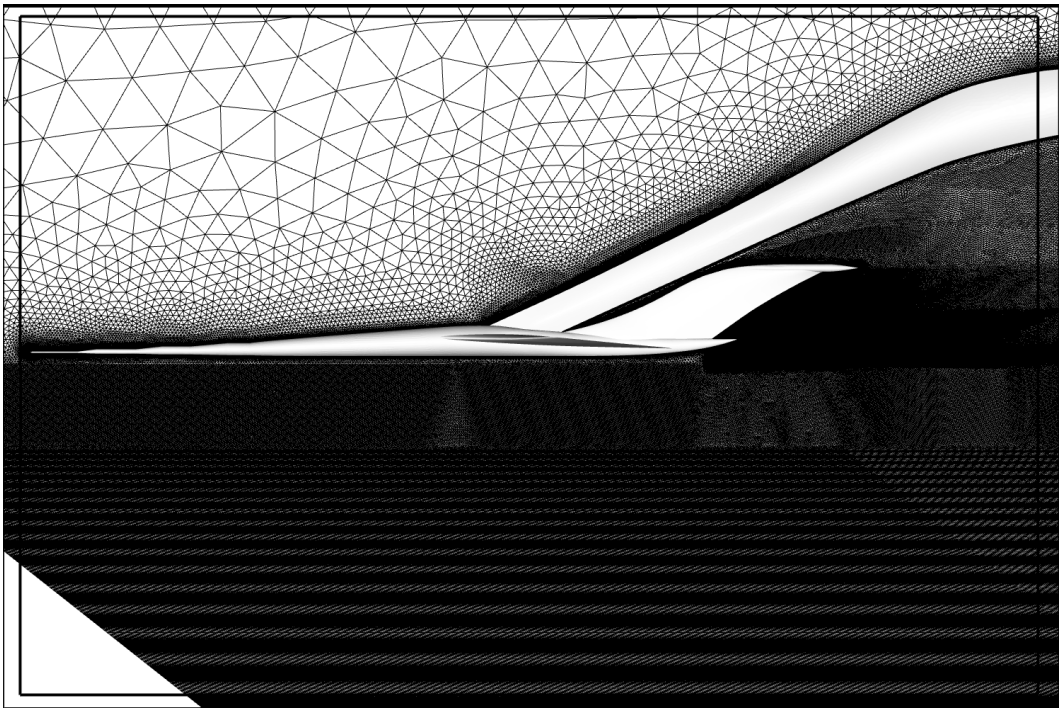

Figure 10. Symmetry plane of the 130 million-cell grid of LBC in free air.

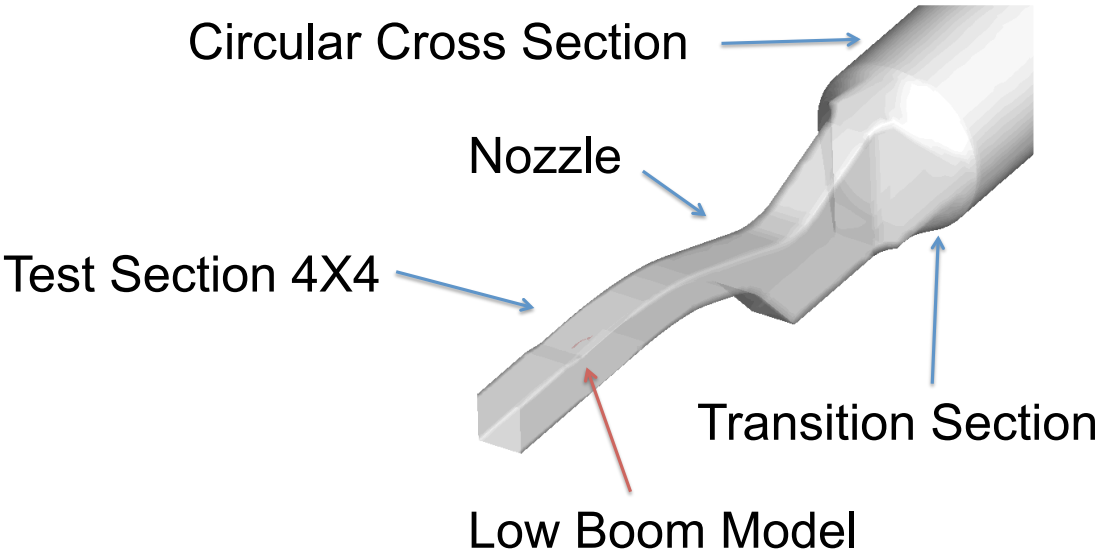

Figure 11. Schematic view of LBC in UPWT.

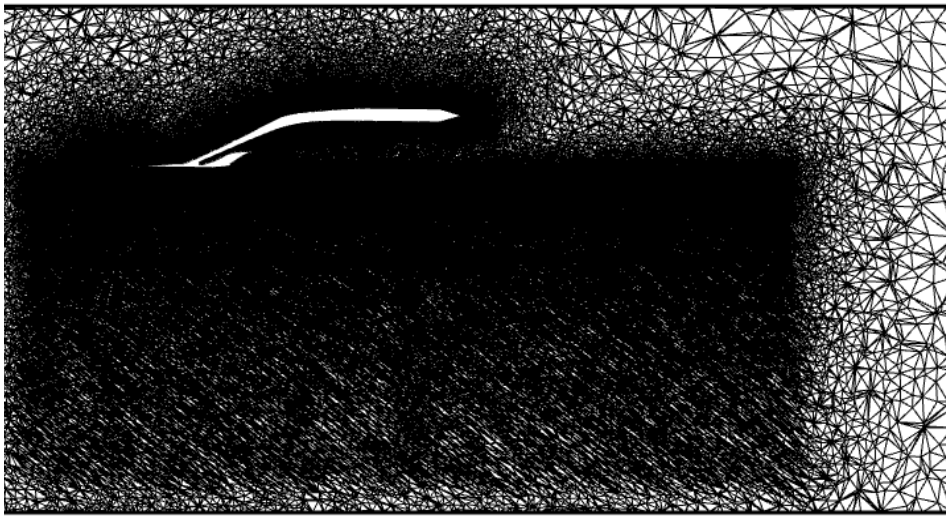

Figure 12. Plane showing distribution of LBC grid inside UPWT.

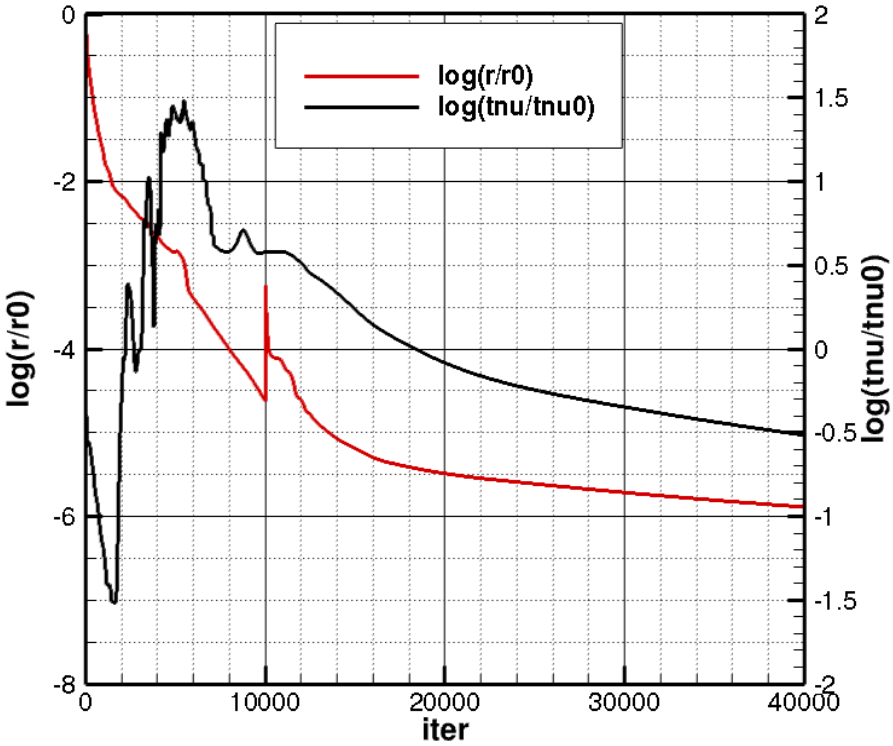

Figure 13. USM3D convergence history.

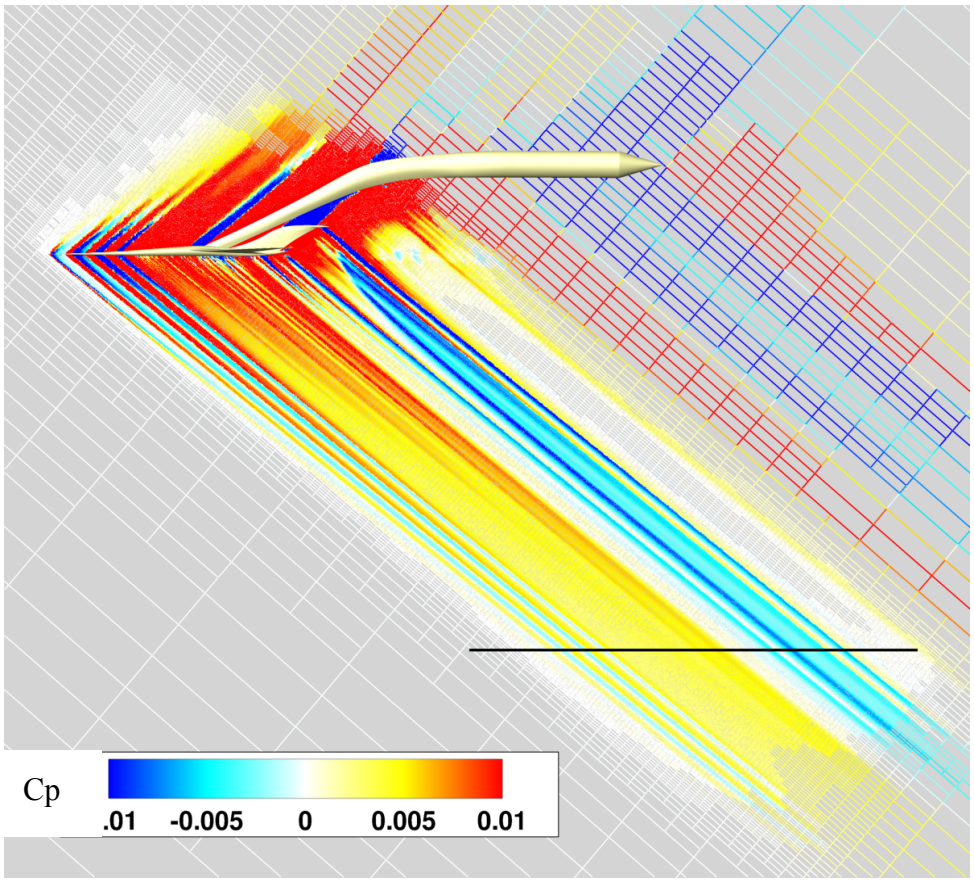

Figure 14. LBC symmetry plane grid colored with Cp.
AERO calculation of the LBC in free air at M=1.6 and ∝= 0.3º.

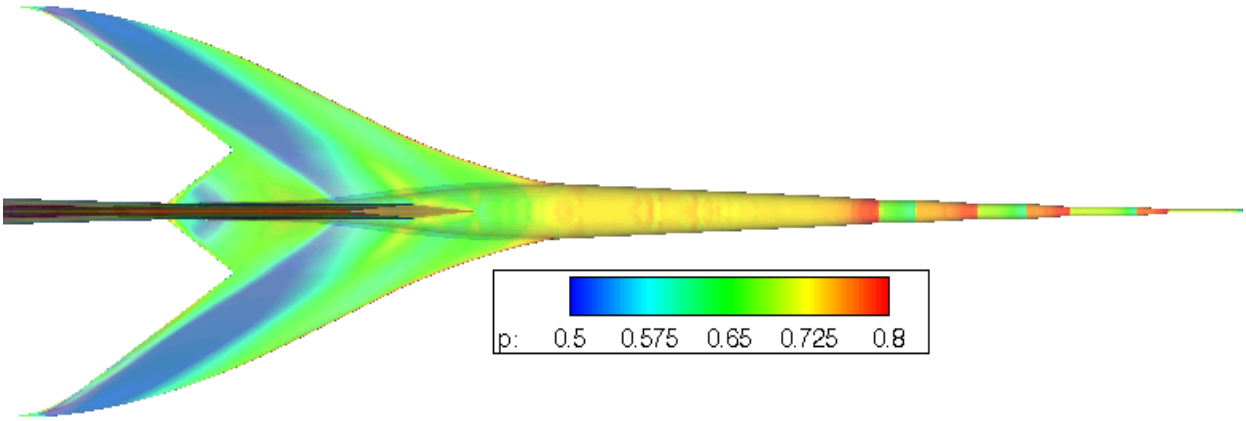

Figure 15. Inviscid pressure distribution on the upper surface.
USM3D inviscid calculation of the LBC in free air at M=1.6 and ∝ = 0.3º.

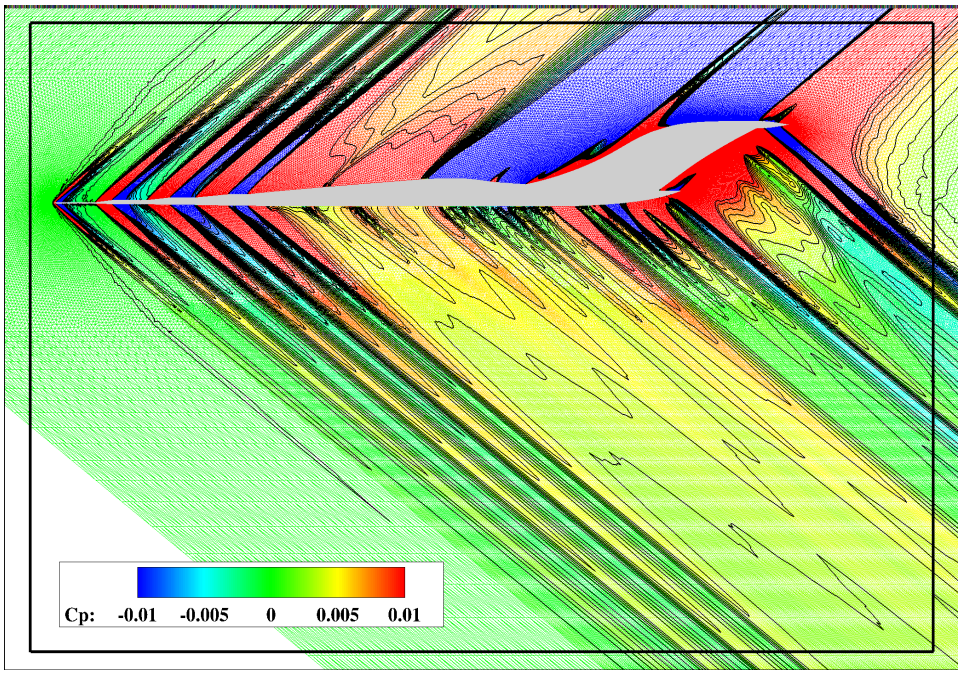

Figure 16. Symmetry plane grid colored by Cp and overlaid with constant pressure lines. USM3D solution of the LBC in free air at M=1.6 and ∝ = 0.3º.

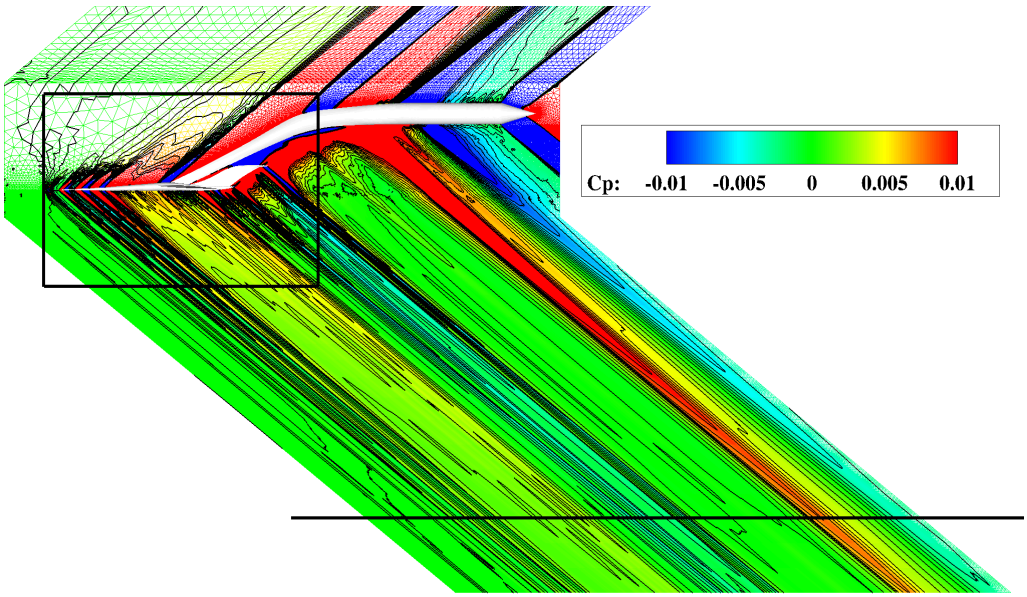

Figure 17. Symmetry plane grid colored by Cp and overlaid with constant pressure lines. USM3D solution of the LBC in free air at M=1.6 and ∝ = 0.3°. Signature sampled at 1.7 body lengths below model.

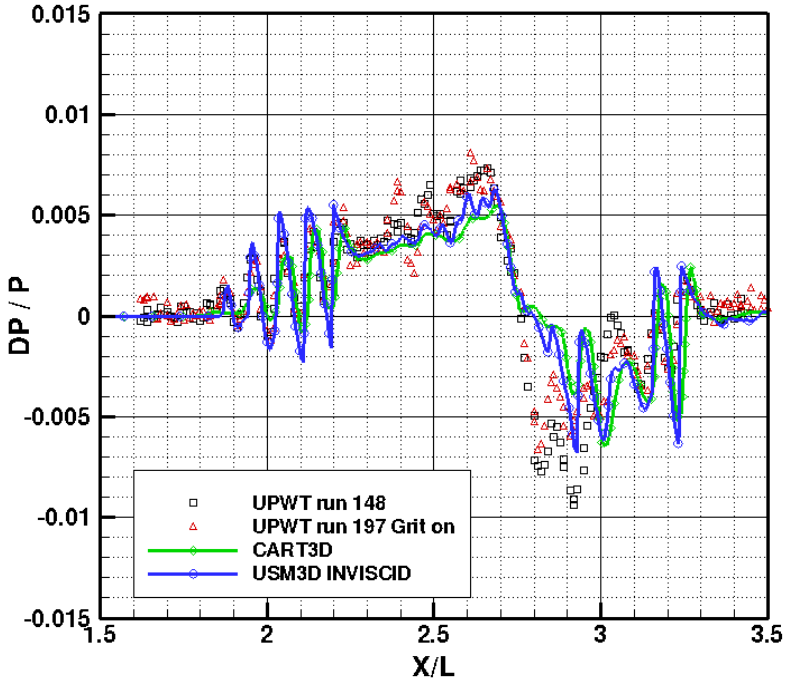

Figure 18. Comparison of inviscid USM3D and AERO data with LARC UPWT data for LBC at M=1.6, $\propto$=0.3°, H/L=1.7, ϕ=0°.

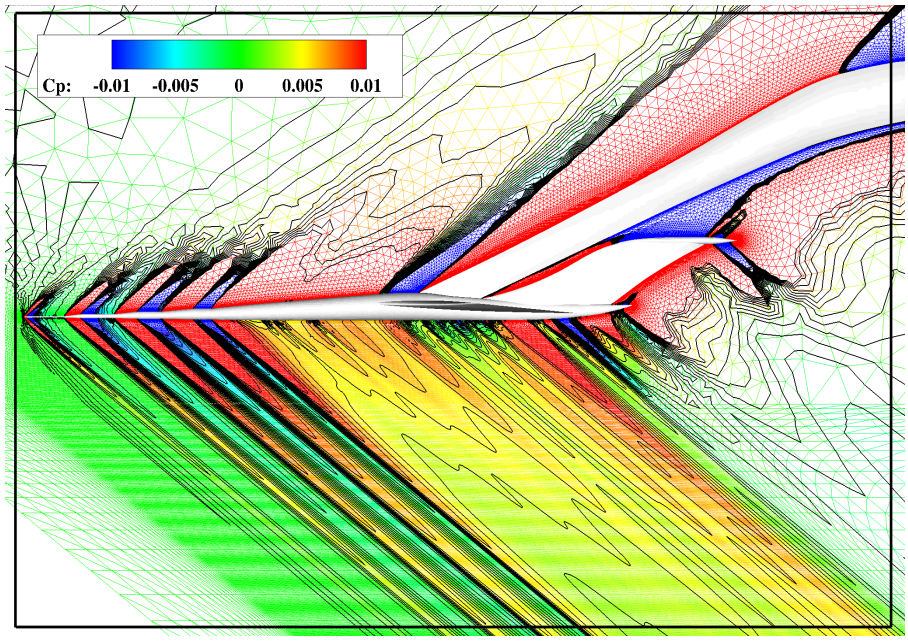

Figure 19. Symmetry plane grid colored by Cp and overlaid with constant pressure lines. USM3D viscous solution of the LBC at M=1.6, $\propto$ = 0.3°, $Re_L = 3.85x10^6$. Grid = 53 million cells.

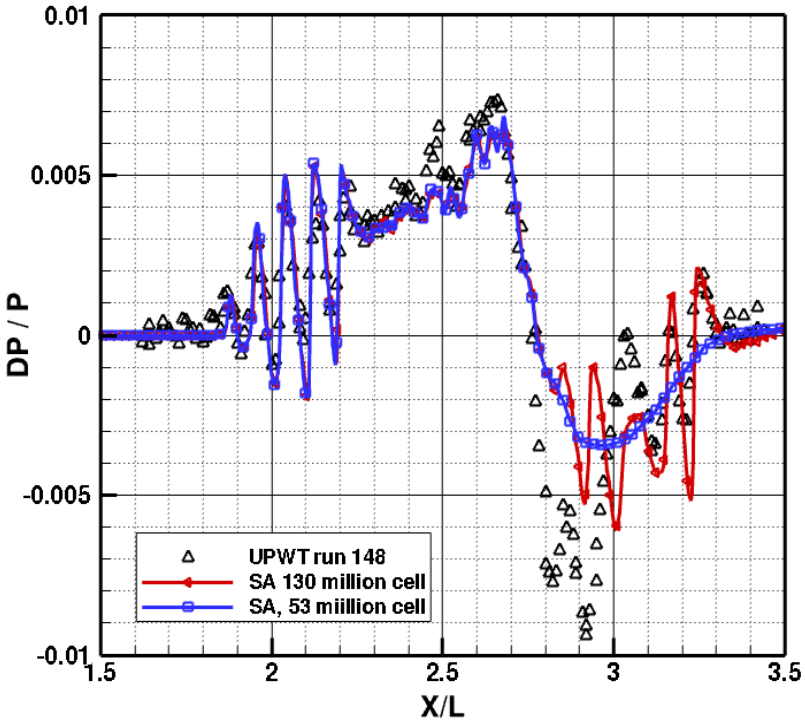

Figure 20. USM3D viscous solution compared with LARC UPWT data at M=1.6, ∝=0.3°, H/L=1.7, $Re_L = 3.85x10^6$, ϕ=0°.

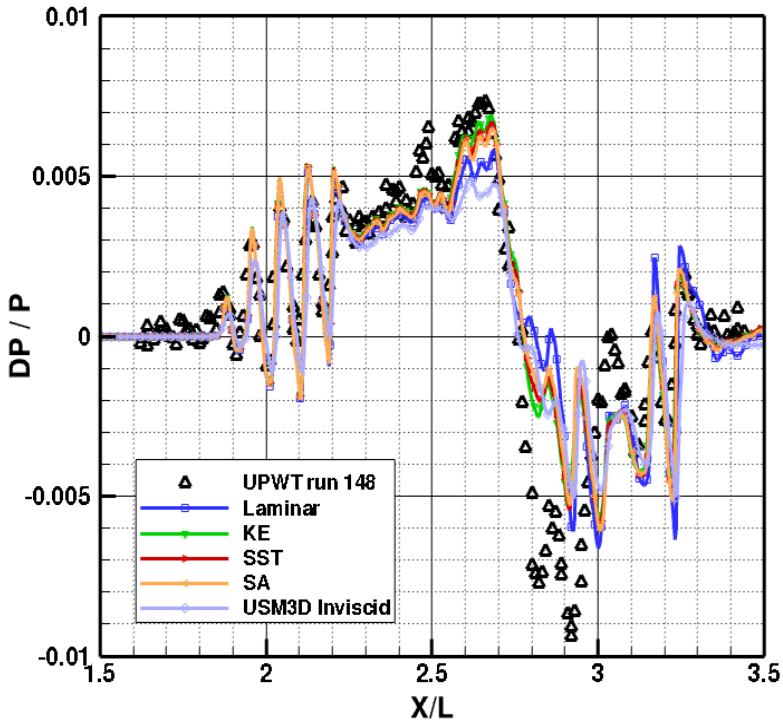

Figure 21. Comparison of USM3D viscous simulations with LARC UPWT data at M=1.6, ∝=0.3°, H/L=1.7, $Re_L = 3.85x10^6$, ϕ = 0°. Grid = 130 million cells.

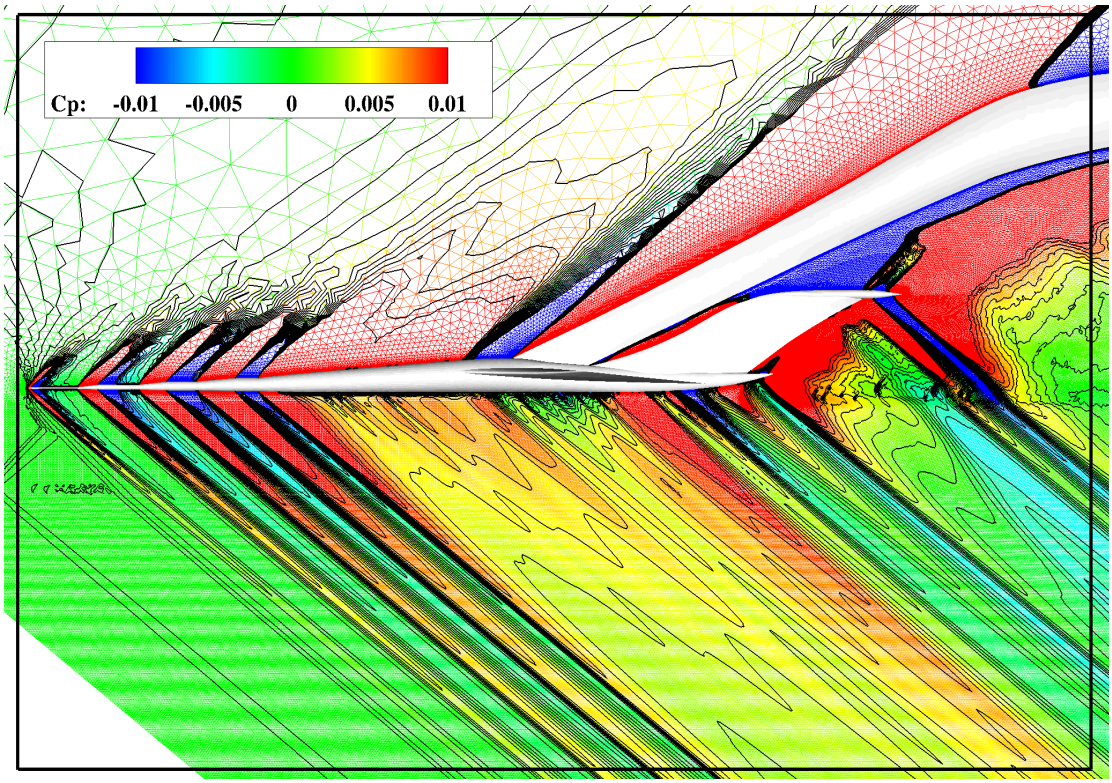

Figure 22. Symmetry plane grid colored by Cp and overlaid with constant pressure lines. USM3D KE solution of the LBC at M=1.6, ∝= 0.3°, $Re_L = 3.85x10^6$. Grid = 130 million cells.

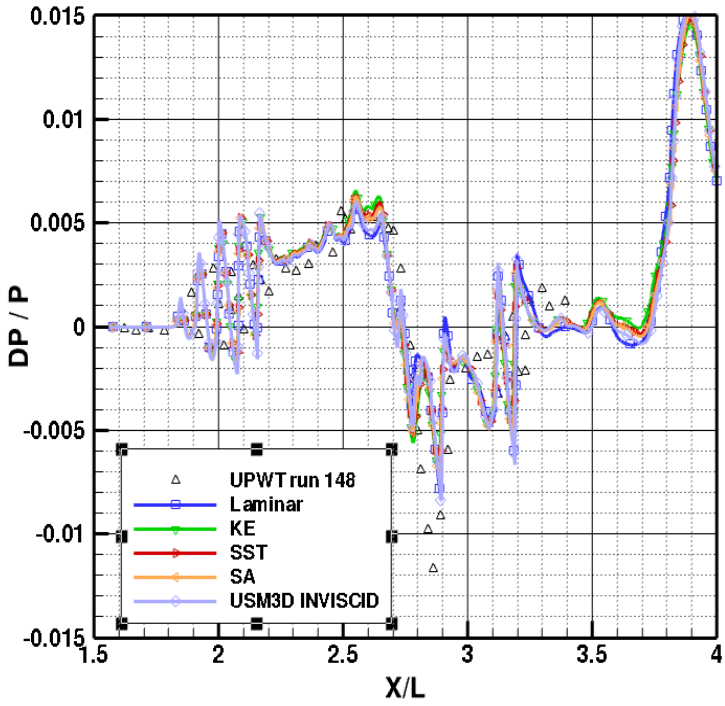

Figure 23. USM3D viscous solution compared with LARC UPWT data at M=1.6, ∝=0.3°, H/L=1.7, $Re_L = 3.85x10^6$, ϕ=20°.

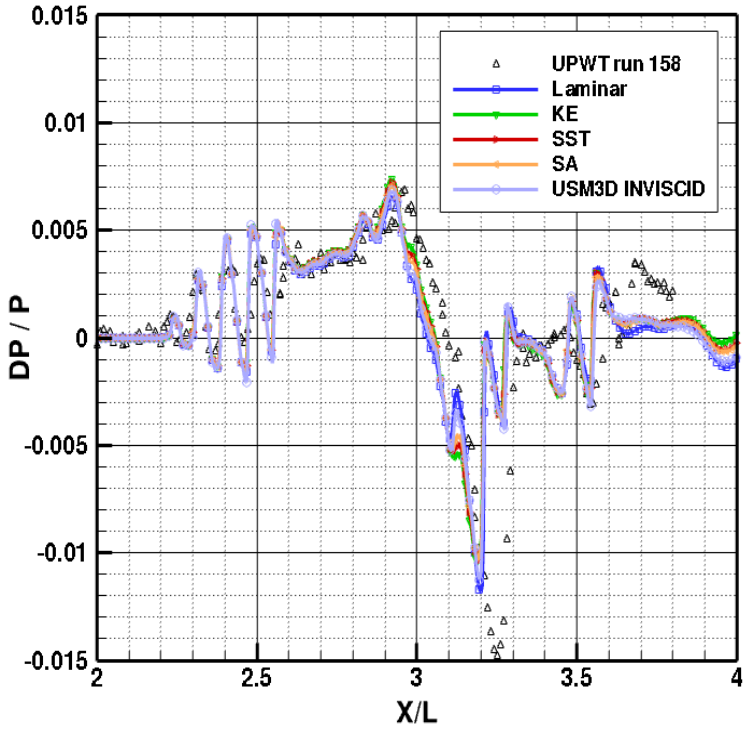

Figure 24. USM3D viscous solution compared with LARC UPWT data at M=1.6, ∝=0.3°, H/L=1.7, $Re_L = 3.85x10^6$, ϕ=45°.

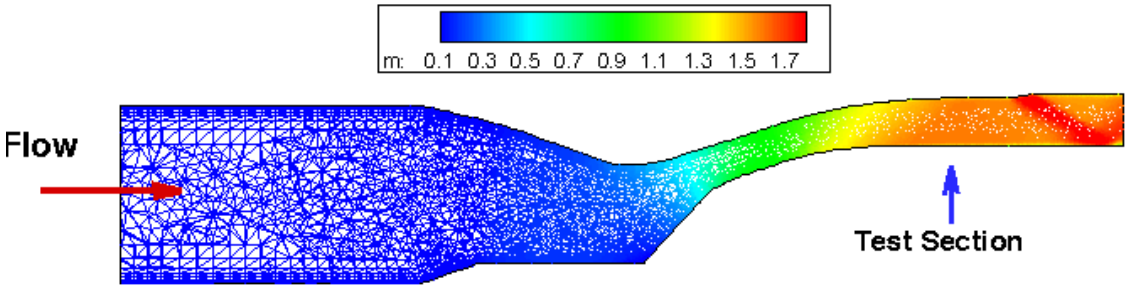

Figure 25. Cross section view of grid colored by Mach contours inside UPWT at M=1.6 and $Re_L = 3.85x10^6$.

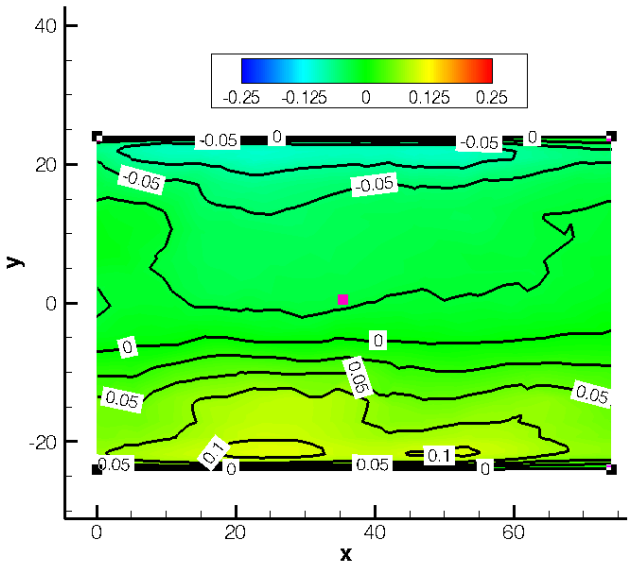

(a) θ_H

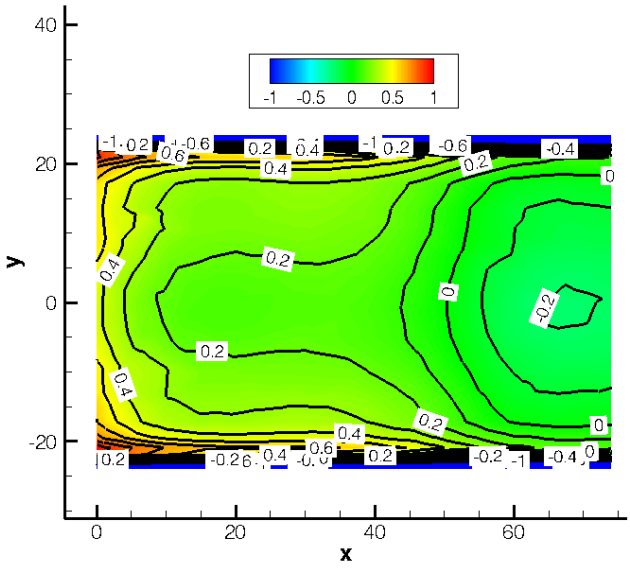

(b) θ_V

Figure 26. Flow angles in the UPWT as computed by USM3D at M=1.6 and $Re_L = 3.85x10^6$ along the Z = 0 plane.

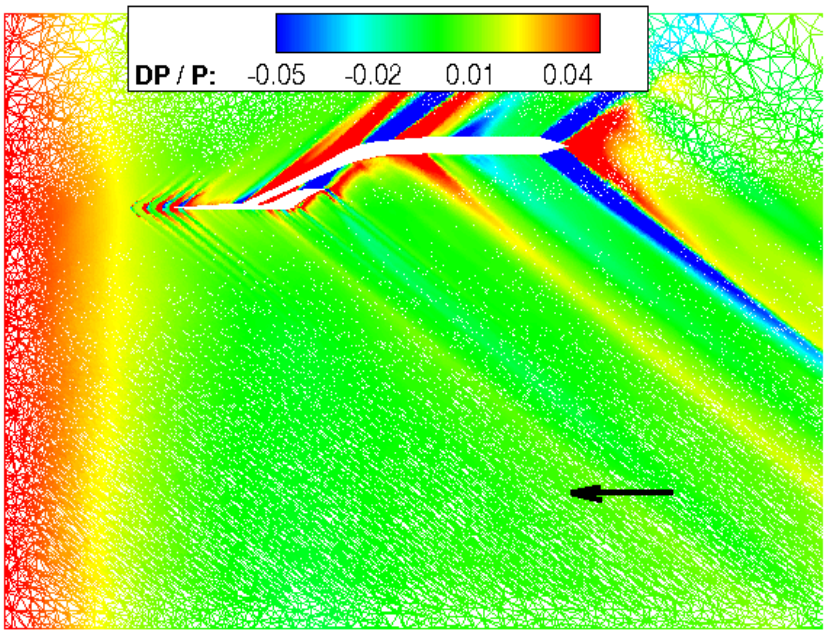

Figure 27 Cross section view of DP/P for LBC inside UPWT at M=1.6, ∝=0.3°, H/L=1.7, $Re_L = 3.85x10^6$. USM3D inviscid solution on a 74 million-cell grid. Arrow points to the location of survey pressure probe.

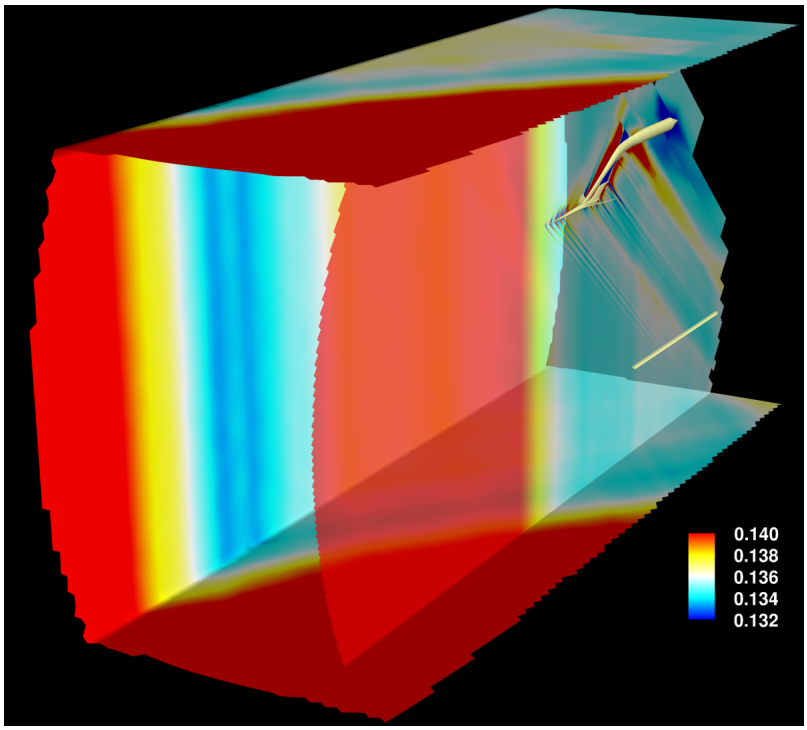

Figure 28. AERO pressure contours of the LBC inside UPWT at M=1.6, ∝=0.3°, H/L=1.7, X_{nose} = 5.0 inches.

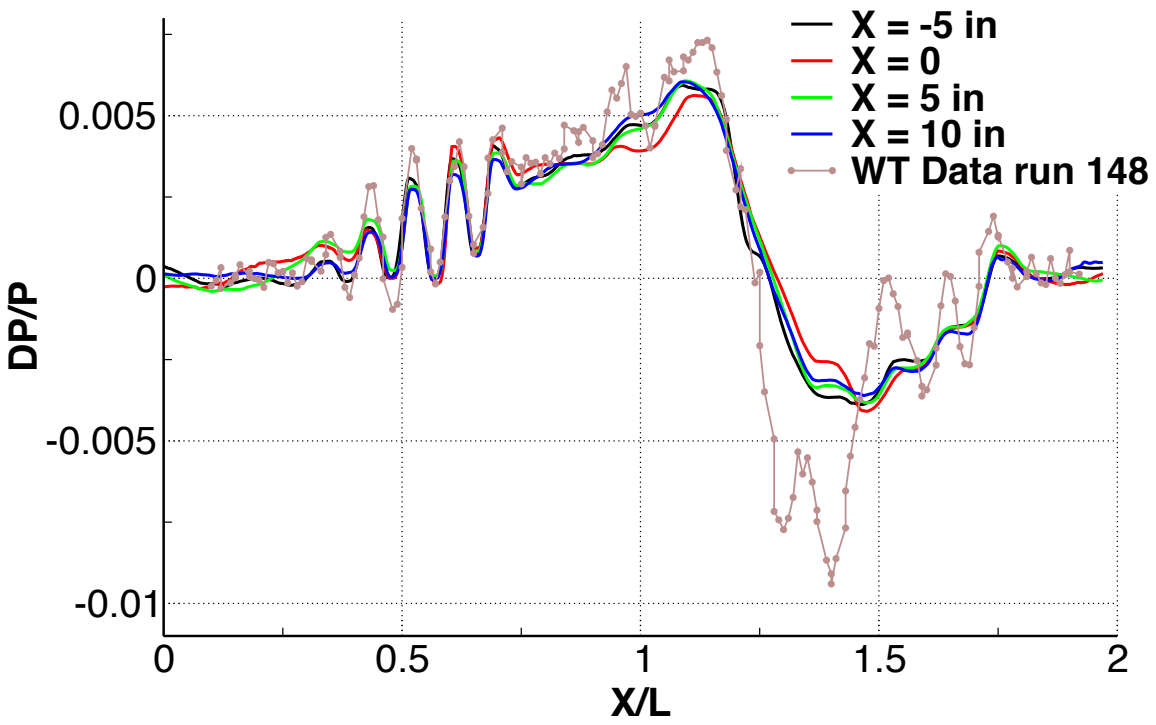

Figure 29. Comparison between AERO computed boom signatures for LBC inside UPWT at M=1.6, ∝=0.3°, H/L=1.7.

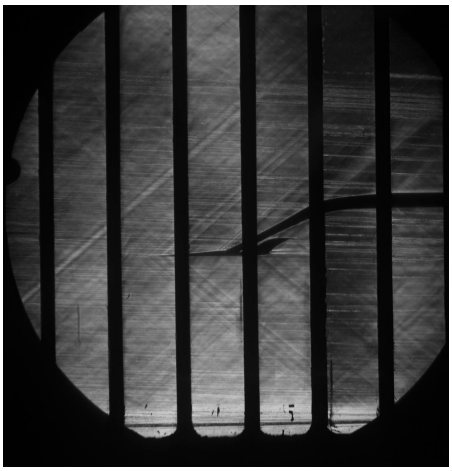

(a) Wind Tunnel Schlieren Images.

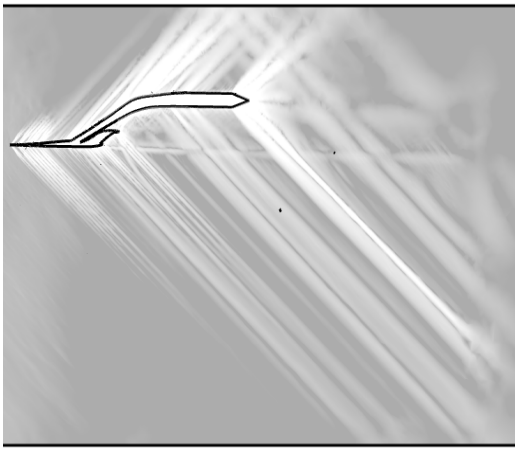

(b) USM3D simulation for LBC in Tunnel.

(c) AERO simulation for LBC in Tunnel.

Figure 30. Comparison of wind tunnel Schlieren images for the LBC inside UPWT and computed density gradients at M = 1.6.